Preprints of the 21st IFAC World Congress (Virtual)
Berlin, Germany, July 12-17, 2020

State Estimation of Material Flow Rate in a Hot Rolling Mill for Steel Bars

Marc-Simon Schaefer * **Juergen Wahrburg** * **Hubert Roth** *

* *Institute of Automatic Control Engineering, University of Siegen, 57076 Siegen, Germany (e-mail: marc-simon.schaefer@uni-siegen.de)*

Abstract: We present a solution for the estimation of the material flow rate for a hot rolling mill for steel bars. In this mill, a high number of uncertainties influences the rolling process. The partly unmeasured flow rate is a critical state for the plant stability. A meaningful estimation increases the operator efficiency. For this, a developed and adapted model of a six-stand finishing mill is used for optimization purpose. The flow rate is estimated with an moving horizon estimator (MHE) with the help of the CasADi framework. The main contribution is the adaption of a simulation model with the usage for online state estimation. The proposed solution is linked with real plant measurements.

Keywords: State estimation, Steel industry, Industry automation, Process models, Moving horizon estimation, System models

1. INTRODUCTION

1.1 Process description

A modern hot rolling mill for steel bars consists out of various stages, beginning with a furnace, roughing stands, intermediate stands and finishing mill (Fig. 1). During these stages, the input material is rolled and reduced in diameter. The material enters in bars of a specific length and is reduced in diameter in a continuous way. The last part – the finishing mill – reduces the diameter to the required output dimension. This finishing mill is a block consisting of numerous roll stands (here $n = 6$). The roll stands are located closely behind each other, which makes the implementation of sensors in between very difficult, because of the reduced space and the harsh environment. In the hot rolling process, there are various process limitations, which impede the application of measurement devices. Material temperatures in the range of 1000 °C, cooling liquid and rough process conditions are leading to high efforts for sensors and their protection. Due to this, only a limited number of measurement signals inside the finishing block are available.

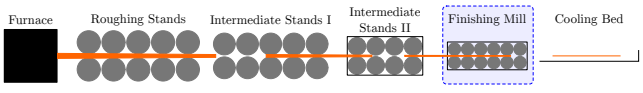

Fig. 1. Overview of components of Hot Rolling Mill with Finishing Mill (blue) as primarily considered object

The six stands create a material coupling between adjoined stands. The action and material deformation of one stand influences the next and the previous. This leads to a coupled process and prevents from investigating the behavior of a single stand.

1.2 Model structure

The finishing mill can be hierarchically structured into several similar stands, with respective own parametrization each Schäfer et al. (2019). A single roll stand is here subdivided into multiple units with its respective basic functionality:

(1) `Motor/Drive`: Simplified motor model, speed controller and drive chain until the work rolls
(2) `Roll Dynamics`: Dynamics of material and work rolls, mechanical friction
(3) `Roll Model`: Static model to calculate roll force, torque, lead of material, material geometry
(4) `Interstand behavior`: Coupling between stands

All submodels contain continuous dynamic systems, only (3) is a nonlinear, time independent static formulation, based on the roll model equations of Lippmann and Mahrenholtz (1967).

1.3 Measurement data

The available measurement data of the process consists of following values:

- Motor torque (each stand)
- Motor speed (actual, reference), (each stand)
- Material velocity (first/last stand)
- Material area (first/last stand)
- Material temperature in/out (first/last stand)
- Roll cylinder position (each stand)

Additionally, there are some process parameters which are time independent, such as roll diameter, roll caliber shape, distances between stands and used materials. The process itself is highly influenced by the kind of material and its chemical composition. This leads to major adaption during process runtime, only because of the resulting strong nonlinear behavior.

These above mentioned signals show, that direct process states of each stand, like input/output material area and velocity are not available as measurements.

1.4 Objectives

The requirements of the process can be divided into two categories. One is the process stability and the other one is the quality of the material output dimension. The output dimension is a result basically of the material reduction of each stand and its roll gap setting. The process stability requires that the material flow rate through the mill is almost constant and without high local deviations. Therefore, a knowledge about the flow rate is crucial. It's a non-measurable value inside of the finishing mill block. But a mismatch can lead to drastic plant failures. There are measurement devices for area and velocity available, but they are very expensive and usually installed only after the last stand of the finishing mill for quality control purpose.

Therefore a robust flow rate estimation is developed to provide these sensitive states for other control stages. Another advantage is, that plant operators can set up faster a scenario with different materials and output dimension, based on the provided internal states. Safety mechanism for unwanted plant behavior, such as *cobbles*, can be more easily detected and a counteraction introduced.

1.5 State of the art

State estimation is a long elaborated research field, starting from observers over estimation algorithms to online optimization methods. The main idea is a more detailed process insight based on some measurements and an internal dynamic model. Additionally, there can be noise characteristics included to obtain a more reliable estimation value.

A comprehensive introduction about existing methods is given by Corriou (2018). There is a general overview about methods, small examples and some remarks about their history. Discussed methods are: Luenberger observer, Kalman Filter (KF), Extended Kalman Filter (EKF), Unscented Kalman Filter (UKF), Ensemble Kalman Filter (EnKF), Particle Filter (PF), High Gain observer and Moving Horizon State Estimation (MHE).

Examples in various applications are found in Dochain (2003), Ritschel and Jorgensen (2018), and Zhang et al. (2014). Also in earlier time multiple research topics were available (Didriksen et al. (1995), Bastin (1990), Soroush (1998)). There are comparisons to handle nonlinear plants with EKF and MHE in Haseltine and Rawlings (2005).

In the steel rolling industry there are also some applied approaches for estimating unmeasurable states. In Rigler et al. (1996) the local temperature and height deviation was obtained from a Kalman filter. McFarlane and Stone (1990) described an EKF for estimating the interstand tension in a finishing mill. Kim et al. (2005) used therefore an Support Vector Regression (SVR) approach. Straub (2013) focused on neural observers in different rolling mill configurations as well as Johansson (2001) did. One major difference between finishing mills setup is the usage of loopers. Loopers are between rolling stands and provide a fast control of the flow rate by introducing a material buffer over the looper arm. With that, changes in the flow rate can be compensated by an underlying control loop. The process described here is without loopers, so there is 1) no material buffer for compensation and 2) no direct knowledge about flow rate changes in between the stands.

The topic of flow rate estimation of different processes is covered in Binder et al. (2015) with an MHE approach, Chhantyal et al. (2018) with an Dynamic Artificial Neural Net and EKF, and Noda and Terashima (2009) with an EKF.

2. PROBLEM FORMULATION

The main task in this work is a robust estimation of the material flow rate throughout all stands in the finishing mill. The flow rate between two stands can be described like in Fig. 2. In general terms it is separated in two regions. First, the control room of the *Deformation zone* under the assumption there is no change of the material flow (1). This zone is assumed as infinitesimal length, leading to a concentrated form by describing it only with input/output behavior:

$$A_0(t) \cdot v_0(t) - A_1(t) \cdot v_1(t) = 0 = const. \tag{1}$$

Where A_0, and A_1 are the material cross-sectional area (input/output), v_0, v_1 the material velocity (input/output). It is valid under the assumption that the material density ρ is constant.

Second, the control room of *Interstand* between two adjoining stands i and $i+1$ with its tensile stress influence. The general volume flow uses the incoming, outgoing and the rate of change according to (2). By inserting the results from (1) of the deformation zone, the effects of the roll model described later are considered.

$$\begin{aligned} \frac{dV_i(t)}{dt} &= A_{1,i}(t) \cdot v_{1,i}(t) - A_{0,i+1}(t) \cdot v_{0,i+1}(t) \\ &= A_{1,i}(t) \cdot v_{1,i}(t) \\ &\quad - A_{0,i+1}(t) \cdot \frac{A_{1,i+1}(t) \cdot v_{1,i+1}(t)}{A_{0,i+1}(t)} \\ A_{1,i}(t) \frac{dL_i(t)}{dt} &= A_{1,i}(t) \cdot v_{1,i}(t) - A_{1,i+1}(t) \cdot v_{1,i+1}(t) \end{aligned} \tag{2}$$

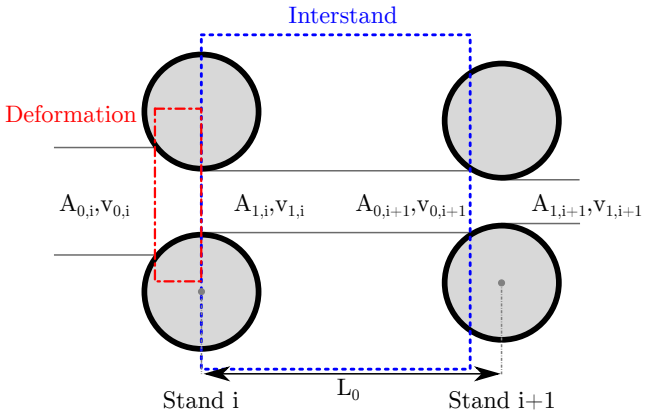

Fig. 2. *Interstand* control room (blue) between to adjoined rolling stands and *Deformation zone* control room (red) at one stand

The elongation between the stands can be expressed with the help of tensile stress σ. The tensile stress or also *tension* has a major impact on the forming process and yields valuable insights in the process safety and quality of the final product.

$$\begin{aligned} \sigma_{0,i+1}(t) &= E \cdot \varepsilon(t) = E \cdot \frac{L_i(t) - L_0}{L_0} \\ \Rightarrow \frac{d\sigma_{0,i+1}(t)}{dt} &= E\frac{d\varepsilon(t)}{dt} = \frac{E}{L_0}\frac{dL_i(t)}{dt} \\ \Rightarrow \frac{dL_i(t)}{dt} &= \frac{L_0}{E}\frac{d\sigma_{0,i+1}(t)}{dt} \end{aligned} \tag{3}$$

Where $\sigma_{0,i+1}$ is the arriving tensile stress of stand $i+1$, ε the elongation in material flow direction, E elastic modulus, L_0 the nominal distance between two stands, and L the elongated length. Inserting (3) in (2) yields:

$$\begin{aligned} A_{1,i}(t)\frac{L_0}{E}\frac{d\sigma_{0,i+1}(t)}{dt} &= A_{1,i}(t) \cdot v_{1,i}(t) \\ &\quad - A_{1,i+1}(t) \cdot v_{1,i+1}(t) \end{aligned} \tag{4}$$

The velocities as well as the cross-sectional areas and tensions are not available as measurements of the intermediate stands. Roll models which describe the static behavior of the forming process are used to calculate the respective nominal values. The geometry change for a three roll equivalent is performed by the proposed method of Overhagen (2018):

$$\underline{\Gamma}_{Out} = \underline{f}_{geom}(\underline{\Gamma}_{In}, \underline{q}) \tag{5}$$

With geometric relevant parameters summarized in $\underline{q}$ and the material state $\underline{\Gamma} = [A, w, h, v, \varphi]^T$ contains: area A, width w, height h, material velocity v, and the reduction ratio φ. The roll model uses the formula by Lippmann and Mahrenholtz (1967):

$$\begin{aligned} [F_R, T_R, \kappa] = \underline{f}_{LM}(&h_0, h_1, b_0, b_1, A_0, A_1, \\ &A_d, l_d, \sigma_0, \sigma_1, r_R, k_{fm}) \end{aligned} \tag{6}$$

Where the subscript 0 indicates input and 1 respectively the output of its variable. The used inputs are a subset of the results obtained by (5) together with the roll radius r_R, pressed area/length A_d, l_d and the mean forming resistance k_{fm}. Additionally, σ_0, σ_1 are the backward / forward material tension. The output F_R is the roll force, T_R the roll torque, and κ the velocity increase to the linear roll velocity v_R with the relation in (7):

$$v_1 = v_R(1 + \kappa) \tag{7}$$

The output area A_1 is calculated with help of the nominal reduction ratio φ in (8):

$$A_{1nom} = \frac{A_0}{exp(\varphi)} \tag{8}$$

Equations (5) and (6) reflect the approximated forming process and yield the required values for the flow rate (A_0,A_1,v_0,v_1). But these equations have some mismatch to the real values and can mostly not be verified with geometric measurements. Therefore, roll force and motor torque are also used as secondary measurements, which are also available as process measurements of each stand.

The above derived formulas are related to a single stand. The finishing block now contains $n = 6$ stands that are coupled. Therefore, a combined representation for $i = 1 \dots n$ is necessary. The state $\underline{x}_i$ is defined as:

$$\underline{x}_i = [v_{1,i}, T_{R,i}, F_{R,i}, A_{1,i}]^T \tag{9}$$

The geometric behavior is highly nonlinear. Due to the fact that these parameters are only slowly changing and the equations are for a static process derived, an artificial smoothing with a first-order term with time constant T_a is introduced (10):

$$\begin{aligned} E(s) &= \frac{1}{T_a s + 1} \\ \Rightarrow \dot{e}(t) &= A(T_a)e(t) + B(T_a)u(t) \end{aligned} \tag{10}$$

With $\underline{A}_{T_a} = A(T_a) \cdot \underline{I}_4$ and $\underline{B}_{T_a} = B(T_a) \cdot \underline{I}_4$, (with $\underline{I}_4$: identity matrix dimension 4) this leads to the expression in (11):

$$\begin{aligned} \underline{f}_i(\underline{x}_i, \underline{u}_i) = \dot{\underline{x}}_i &= \begin{bmatrix} \dot{v}_{1,i} \\ \dot{T}_{R,i} \\ \dot{F}_{R,i} \\ \dot{A}_{1,i} \end{bmatrix} \\ &= \underline{A}_{T_a} \cdot \underline{x}_i + \underline{B}_{T_a} \cdot \begin{bmatrix} v_{R,i} \cdot (1 + \kappa_i) \\ T_{R,i} \\ F_{R,i} \\ A_{1nom,i} \end{bmatrix} \end{aligned} \tag{11}$$

The inputs of each stand are defined in (12) as:

$$\underline{u}_i = \left[v_{0,i}, A_{0,i}, k_{fm,i}, \varphi_i, \sigma_{0,i}, \sigma_{1,i}, \underline{p}_i\right]^T \tag{12}$$

The coupling between the stands results in a shift of the variables for $i \in 1 \dots 5$ (13):

$$\begin{aligned} A_{0,i+1} &= A_{1,i} \\ v_{0,i+1} &= v_{1,i} \\ \sigma_{0,i+1} &= \sigma_{1,i} \end{aligned} \tag{13}$$

The entire problem is combined into a summarized state space representation (14) denoted with *hat* ($\hat{\cdot}$) with the previously introduced relationships:

$$\begin{aligned} \hat{\underline{f}}(\hat{\underline{x}}, \hat{\underline{u}}) &= \begin{bmatrix} \underline{f}_1(\underline{x}_1, \underline{u}_1) \\ \vdots \\ \underline{f}_6(\underline{x}_6, \underline{u}_6) \end{bmatrix} \\ \hat{\underline{x}} &= [\underline{x}_1 \dots \underline{x}_6]^T \\ \hat{\underline{u}} &= [\underline{u}_1 \dots \underline{u}_6]^T \end{aligned} \tag{14}$$

3. METHOD DESCRIPTION

As described in the previous section, we have to consider various parts in our problem formulation:

(1) Nonlinear coupled state space system
(2) Constraints, due to mass conservation and coupling

Therefore, we propose a Moving Horizon Estimator (MHE) for solving this task. Especially the conservation laws and state restrictions led to this decision. In general it is described by a Optimal Control Problem (OCP) formulation in the following form:

$$\begin{aligned} &\underset{\hat{\underline{x}}, \hat{\underline{u}}, \underline{w}}{\operatorname{argmin}} J(\hat{\underline{x}}, \hat{\underline{u}}, \underline{w}, \underline{p}) \\ s.t.\ &\hat{\underline{x}}(j+1) = \hat{\underline{f}}(\hat{\underline{x}}(j), \hat{\underline{u}}(j)) + \underline{w}(j), \\ &\hat{\underline{x}}(k-N) = \hat{\underline{x}}_0, \\ &\hat{\underline{u}}(j) \in U, \forall j \in [k-N, k-1] \\ &\hat{\underline{x}}(j) \in X, \forall j \in [k-N, k] \end{aligned} \tag{15}$$

$$\begin{aligned}\text{with: } J(\underline{\hat{x}},\underline{\hat{u}}) &= ||\underline{\hat{x}}_0 - \underline{\hat{x}}(k-N)||^2_{\underline{S}} \\ &+ \sum_{j=k-N}^{k} ||\underline{\tilde{y}}(j) - \underline{h}(\underline{\hat{x}}(j))||^2_{\underline{Q}} \\ &+ \sum_{j=k-N}^{k-1} ||\underline{\tilde{u}}(j) - \underline{\hat{u}}(j)||^2_{\underline{R}} \\ &+ \sum_{j=k-N}^{k-1} ||\underline{w}(j)||^2_{\underline{D}}\end{aligned} \tag{16}$$

With: $\underline{\tilde{u}}$ the past inputs, $\underline{h}$ the output equations, $\underline{\tilde{y}}$ the past measurements, and $\underline{w}$ the unknown, additive process noise. The weighting matrices $\underline{S}$, $\underline{Q}$, $\underline{R}$, and $\underline{D}$ are chosen as diagonal matrices with only positive values to ensure their positive definite property. The system representation is converted from a continuous representation ($\underline{\dot{\hat{x}}}(t)$) to a discrete one ($\underline{\hat{x}}(k+1)$) by using trapezoidal integration.

This OCP is solved with CasADi toolbox (Joel A E Andersson et al. (2019)) by using a Multiple Shooting (MS) algorithm to transform it into a Nonlinear Program (NLP).

$$\begin{aligned}&\underset{\underline{\omega}}{\operatorname{argmin}}\, J(\underline{\omega},\underline{p}) \\ &s.t. \quad \underline{\omega}_{lb} \le \underline{\omega} \le \underline{\omega}_{ub} \\ &\qquad \underline{g}_{lb} \le \underline{g}(\underline{\omega},\underline{p}) \le \underline{g}_{ub}\end{aligned} \tag{17}$$

Where $\underline{g}_{lb,ub}$ are the (in)equality constraints and $\underline{\omega}_{lb,ub}$ the state constraints. The decision variable $\underline{\omega}$ combines the states, inputs and disturbances (18):

$$\underline{\omega} = [\underline{\hat{x}}, \underline{\bar{u}}, \underline{w}]^T \tag{18}$$

The inputs $\underline{\bar{u}}$ extract only the inputs from $\underline{\hat{u}}$ which are not derived by the shifted solution in (13).

$$\begin{aligned}\underline{\bar{u}} = [&A_0, v_0, k_{fm,1} \dots k_{fm,6}, \varphi_1 \dots \varphi_6, \\ &\sigma_{0,1} \dots \sigma_{0,6}, \sigma_{1,6}]\end{aligned} \tag{19}$$

The output function $\underline{h}$ returns a subset of the states $\underline{\hat{x}}$:

$$\underline{\tilde{y}} = \underline{h}(\underline{\hat{x}}) = [F_{R,1} \dots F_{R,6}, T_{R,1} \dots T_{R,6}, A_{1,6}, v_{1,6}] \tag{20}$$

The block diagram of the used MHE structure is shown in Fig. 3. The entire MHE algorithm can be enabled after the

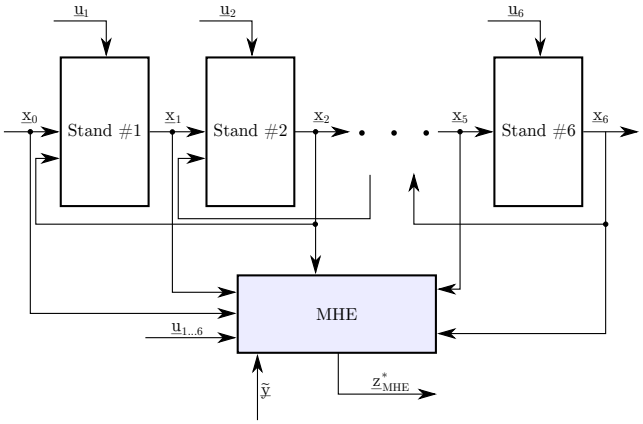

Fig. 3. Overview of MHE structure combined with model outputs $\underline{x}_i$, measurement values $\underline{\tilde{y}}$, and its estimated output $\underline{z}^*_{MHE}$

bar entered *all* stands. After that, a measurement value for the output speed and area are available for correction.

In the problem formulation are following constraints considered:

$$\begin{aligned}&1) && \underline{\hat{x}}(j+1) - \underline{\hat{f}}(\underline{\hat{x}},\underline{\hat{u}}) = 0 \\ &2) && v_{0,i} - v_{R,i} \le 0 \\ &3) && v_{R,i} - v_{1,i} \le 0 \\ &4) && v_{1,i}A_{1,i} - v_{1,i+1}A_{1,i+1} - A_{1,i}\frac{L_0}{E}\frac{d\sigma_{0,i+1}}{dt} = 0\end{aligned} \tag{21}$$

The constraint 1) is for the Multiple Shooting to ensure smoothness of states at the sample time steps. The constraints 2) and 3) are for ensuring the material speed increases through the stands. Constraint 4) implements the volume flow balance (implicit version of (4)).

The decision variable $\underline{\omega}$ is scaled so that all values are in the range of approx. $0.1 \dots 10$. This provides better numerical accuracy especially with very small/large numbers due to physical units.

4. PARAMETRIZATION

The general plant parameters are set accordingly to a real plant under investigation in this project. Parameters like roll properties, geometric bounds, and material properties are extracted from the plant configuration logs.

4.1 Scenario preparation

The plant data acquisition system provides an insight in many plant-wide states such as e.g. motor torque, speed, roll force. Additionally, there is a high precision online measurement for the speed and shape located after the last stand. In front of the first stand is a rough area measurement located. The different data sources are time-aligned to get a common dataset. After that, a simulation (Schäfer et al. (2019)) of the roll process is executed to get an approximated overview of the expected outputs of each stand. In particular the geometric behavior is important during that stage. This result is fed into a static optimization of the tensions in between the stands. The dataset is augmented by these values and provides the initial set for the used scenarios. During these steps it is known that various uncertainties and errors are included into the dataset.

4.2 MHE Parameters

The simulation is calculated with a sample rate of $T_s = 0.001\,\text{s}$. The MHE has a slower sample time of $T_{MHE} = 0.1\,\text{s}$. This value was increased to lower the computational load and addresses the reduced update rate of some measurement values. The estimation horizon was set to $N_{MHE} = 30$ steps. The weighting matrices for the cost function (16) are scaled identity matrices (Note: the expression $(0.1)_{n,T_R}$ indicates n times the weight of state T_R).

The measurements are weighted with:

$$\underline{Q} = diag([(0.01)_{n,T_R}, (0.1)_{n,F_R}, 2_{v_{0,1}}, 5_{A_{0,1}}]) \tag{22}$$

The input weighting:

$$\underline{R} = diag([1_{v_{0,1}}, 2_{A_{0,1}}, (1)_{n,k_{fm}}, (0.1)_{n,\varphi}, (1)_{n,\sigma_0}, 0.1_{\sigma_{1,6}}]) \tag{23}$$

The arrival cost is implemented as a fixed weighting:

$$\underline{S} = diag([(1)_{n,v_1}, (0.01)_{n,T_R}, (0.1)_{n,F_R}, (10)_{n,A_1}]) \quad (24)$$

The process noise uses following values for all stands:

$$\underline{D} = diag([(1)_{n,v_1}, (0.0025)_{n,T_R}, (0.04)_{n,F_R}, (1)_{n,A_1}]) \quad (25)$$

In fact of the scaling in the NLP formulation, the weights can be adjusted as relative values independent of the magnitude of the actual variable. This leads to an increased comparability between the values and their influence in the overall cost function.

In summary, the measured area and velocity get a higher significance, because they yield direct insight into the flow rate. Whereas the torque is more uncertain because of some measurement noise as well as unknown friction coefficients.

For all decision variables $\underline{\omega}$ a state constraint could be set. Here, the states and inputs are limited to process relevant ranges, whereas the noise parameters kept unconstrained (Table 1).

Table 1. Decision variable constraints

Value	Unit	lower limit	upper limit
$v_{1,i}$	$[m/s]$	1	15
$T_{R,i}$	$[Nm]$	−50000	50000
$F_{R,i}$	$[kN]$	0	400
$A_{1,i}$	$[mm^2]$	1	2000
$v_{0,1}$	$[m/s]$	1	10
$A_{0,1}$	$[mm^2]$	1	2000
$k_{fm,i}$	$[N/mm^2]$	1	300
φ_i	[1]	eps	1
$\sigma_{0,i}$	$[N/mm^2]$	−200	200
$\sigma_{1,6}$	$[N/mm^2]$	−200	200
$\underline{w}$	[1]	-inf	inf

5. SIMULATION RESULTS

For the simulation the MATLAB/Simulink implementation of the six stand roll model described in Schäfer et al. (2019) is used. It uses also the inputs from the plant data acquisition. The simulation stability is achieved by using a tension PI-controller. Under the condition that model errors are inevitable, the controller adapts κ (indirect output speed $v_{1,i}$) to bring stability with the given boundaries and minimizes the tension.

In Fig. 4 the input/output areas are shown. The output estimation follows the measurement very precisely. The assumed input area has some deviations, that the input uncertainty of the MHE accounts for. The nominal simulated output area diverges from the measurement by approx. 8 %.

The related material velocities are shown in Fig. 5. Here is also a close match between the measurements and the output estimation. The simulation leads also to a mismatch of approx. 8 %. This coincides with the results of the area above. The simulation itself is stable, so that a mismatch to a constant flow rate is automatically compensated for, but to different absolute values. The initial delay between estimation result and measurements at $t \approx 20$ s is the time the MHE buffer has to fill, before a calculation is performed.

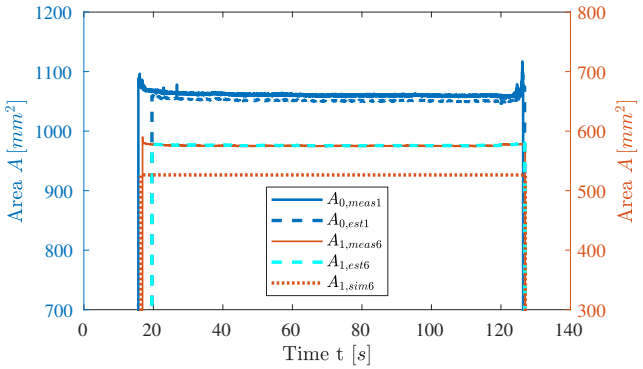

Fig. 4. Estimated and measured input area (blue) together with measured, simulated, and estimated output area (red, cyan)

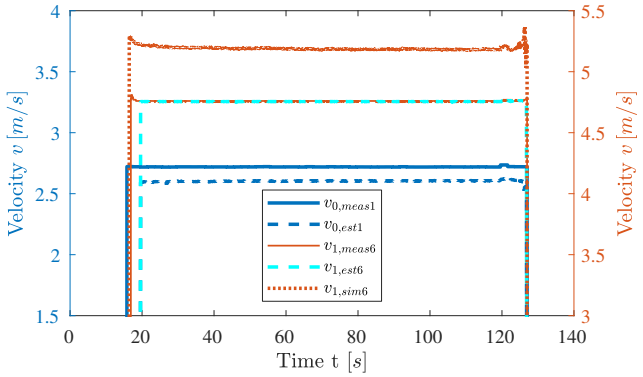

Fig. 5. Estimated and measured input velocity (blue) together with measured, simulated, and estimated output velocity (red, cyan)

Not only the flow rate, but also roll forces and torques are relevant in the entire MHE optimization. The Tables 2 and 3 show the average roll torque and force between estimation and measured values for each stand. The MHE model includes also a noise component for each state, which indicates how accurate the model description with the given parameters is.

Table 2. Roll Torque deviation (Average)

Stand	#1	#2	#3	#4	#5	#6
$T_{R,meas}$ [Nm]	1579	6547	7010	7848	1642	385
$T_{R,est}$ [Nm]	1708	6577	7256	8043	1605	301
$T_{R,noise}$ [Nm]	-805	-401	-1192	-608	351	507
Error_{Est} [%]	8.22	0.45	3.51	2.49	-2.22	-21.88

Table 3. Roll Force deviation (Average)

Stand	#1	#2	#3	#4	#5	#6
$F_{R,meas}$ [kN]	119	145	64	111	86	54
$F_{R,est}$ [kN]	124	143	64	106	77	51
$F_{R,noise}$ [kN]	-15	1	-1	12	20	7
Error [%]	4.27	-1.37	-0.57	-4.61	-9.68	-5.01

The deviation of force and torque indicates that some modeling errors exist. Especially the first and last stand have bigger differences between estimation and measured values in the roll torque. The noise influence is also higher in the roll torque, which indicates some unmodeled behavior in these stands.

6. CONCLUSION

In this work we presented an application of a Moving Horizon Estimator (MHE) for solving the flow rate estimation in a hot rolling finishing mill. We obtained the results by using plant measurements and applied the algorithm offline in our simulation. The results showed a error minimization of the model states to the measurements of material area and velocity as well their influence in roll torque and force. The MHE refines the simulation model output and decreases the model mismatch with online data. Based on these boundary conditions it provides also insight into the non-measurable interstand values such as area and velocity.

A next step is to find a maximum acceptable computation time to enable the algorithms on a real-time device. With that, an online estimation during the real process is possible and delivers valuable insights. The future work contains also the verification on additional materials and plant setups.

ACKNOWLEDGEMENTS

This work was done under the PIREF project. The PIREF research project is funded by the European Regional Development Fund (EFRE) from 2017 to 2020.

REFERENCES

Bastin, G. (1990). *On-line Estimation and Adaptive Control of Bioreactors*. Process Measurement and Control. Elsevier Science, Burlington.

Binder, B.J., Pavlov, A., and Johansen, T.A. (2015). Estimation of Flow Rate and Viscosity in a Well with an Electric Submersible Pump using Moving Horizon Estimation. *IFAC-PapersOnLine*, 48(6), 140–146. doi:10.1016/j.ifacol.2015.08.022.

Chhantyal, K., Hoang, M., Viumdal, H., and Mylvaganam, S. (2018). Flow Rate Estimation using Dynamic Artificial Neural Networks with Ultrasonic Level Measurements. In *Proceedings of The 9th EUROSIM Congress on Modelling and Simulation, EUROSIM 2016, The 57th SIMS Conference on Simulation and Modelling SIMS 2016*, Linköping Electronic Conference Proceedings, 561–567. Linköping University Electronic Press. doi:10.3384/ecp17142561.

Corriou, J.P. (2018). *Process Control: Theory and Applications*. Springer International Publishing, Cham, 2nd edition 2018 edition.

Didriksen, H., Hillestad, M., Andersen, K.S., and Balchen, J.G. (1995). State and Parameter Estimation with Augmented Kalman Filter Applied to an Industrial Polymer Reactor. *IFAC Proceedings Volumes*, 28(9), 281–285. doi:10.1016/S1474-6670(17)47050-9.

Dochain, D. (2003). State observers for processes with uncertain kinetics. *International Journal of Control*, 76(15), 1483–1492. doi:10.1080/00207170310001604936.

Haseltine, E.L. and Rawlings, J.B. (2005). Critical Evaluation of Extended Kalman Filtering and Moving-Horizon Estimation. *Industrial & Engineering Chemistry Research*, 44(8), 2451–2460. doi:10.1021/ie034308l.

Joel A E Andersson, Joris Gillis, Greg Horn, James B Rawlings, and Moritz Diehl (2019). CasADi – A software framework for nonlinear optimization and optimal control. *Mathematical Programming Computation*, 11(1), 1–36. doi:10.1007/s12532-018-0139-4.

Johansson, A. (2001). *Nonlinear observers with applications in the steel industry*. Doctoral thesis, Department of Computer Science and Electrical Engineering, Lulea, Sweden.

Kim, J.D., Shim, J.H., Han, D.C., Park, C.J., Park, H.D., and Lee, S.G. (2005). A study of tension control in looperless hot rolling process using SVR. In Y. Wei, K.T. Chong, T. Takahashi, S. Liu, Z. Li, Z. Jiang, and J.Y. Choi (eds.), *ICMIT 2005: Control Systems and Robotics*, SPIE Proceedings, 60420Z. SPIE. doi:10.1117/12.664582.

Lippmann, H. and Mahrenholtz, O. (1967). *Plastomechanik der Umformung metallischer Werkstoffe: Erster Band*. Springer Berlin Heidelberg, Berlin, Heidelberg.

McFarlane, D.C. and Stone, P.M. (1990). Minimum Tension in a Merchant Bar Rolling Mill using Modern Control Techniques. *IFAC Proceedings Volumes*, 23(8), 137–142. doi:10.1016/S1474-6670(17)51409-3.

Noda, Y. and Terashima, K. (2009). Estimation of flow rate in automatic pouring system with real ladle used in industry. In *2009 ICCAS-SICE*, 354–359.

Overhagen, C. (2018). *Modelle zum Walzen von Flach- und Vollquerschnitten*. Ph.D. thesis, Universität Duisburg-Essen.

Rigler, G.W., Aberl, H.R., Staufer, W., Aistleitner, K., and Weinberger, K.H. (1996). Improved rolling mill automation by means of advanced control techniques and dynamic simulation. *IEEE Transactions on Industry Applications*, 32(3), 599–607. doi:10.1109/28.502172.

Ritschel, T.K.S. and Jorgensen, J.B. (2018). Nonlinear Filters for State Estimation of UV Flash Processes. In *2018 IEEE Conference on Control Technology and Applications (CCTA)*, 1753–1760. IEEE, Piscataway, NJ. doi:10.1109/CCTA.2018.8511532.

Schäfer, M.S., Gamal, O., Wahrburg, J., and Roth, H. (2019). Modellierung, Parameterschätzung und Validierung eines Warmwalzprozesses für Draht und Stabstahl am Beispiel eines realen Walzwerks. In *Automation 2019*, VDI-Berichte, 1035–1046. VDI Verlag GmbH, Düsseldorf.

Soroush, M. (1998). State and parameter estimations and their applications in process control. *Computers & Chemical Engineering*, 23(2), 229–245. doi:10.1016/S0098-1354(98)00263-4.

Straub, S.O. (2013). *Entwurf und Validierung neuronaler Beobachter zur Regelung nichtlinearer dynamischer Systeme im Umfeld antriebstechnischer Problemstellungen*. Elektrotechnik. Herbert Utz Verl., München, 2., unveränd. aufl. edition.

Zhang, J., Welch, G., Bishop, G., and Huang, Z. (2014). A Two-Stage Kalman Filter Approach for Robust and Real-Time Power System State Estimation. *IEEE Transactions on Sustainable Energy*, 5(2), 629–636. doi:10.1109/TSTE.2013.2280246.